

Supramolecular Structures and Photoelectronic Properties of the Inclusion Complex of a Cyclic Free-Base Porphyrin Dimer and C₆₀

Hirofumi Nobukuni,^[a] Yuichi Shimazaki,^[b] Hidemitsu Uno,^[c] Yoshinori Naruta,^[a] Kei Ohkubo,^[d] Takahiko Kojima,^[e] Shunichi Fukuzumi,^[d, f] Shu Seki,^[g] Hayato Sakai,^[h] Taku Hasobe,^[h] and Fumito Tani^{*,[a]}

Abstract: A cyclic free-base porphyrin dimer H₄-CPD_{py} (CPD=cyclic porphyrin dimer) linked by butadiyne moieties bearing 4-pyridyl groups self-assembles to form a novel porphyrin nanotube in the crystalline state. The cyclic molecules link together through non-classical C–H···N hydrogen bonds and π–π interactions of the pyridyl groups along the crystallographic *a* axis. H₄-CPD_{py} includes a C₆₀ molecule in its cavity in solution. In the crystal structure of the inclusion complex (C₆₀⊂H₄-CPD_{py}), the dimer “bites” a C₆₀ molecule by tilting the porphyrin rings with respect to each other, and there are strong π–π interactions between the

porphyrin rings and C₆₀. The included C₆₀ molecules form a zigzag chain along the crystallographic *b* axis through van der Waals contacts with each other. Femtosecond laser flash photolysis of C₆₀⊂H₄-CPD_{py} in the solid state with photoexcitation at 420 nm shows the formation of a completely charge-separated state {H₄-CPD_{py}^{•+} + C₆₀^{•-}}, which decays with a lifetime of 470 ps to the ground state.

Keywords: charge transfer • fullerenes • photoinduced electron transfer • photovoltaics • porphyrinoids

The charge-carrier mobility of the single crystal of C₆₀⊂H₄-CPD_{py} was determined by flash photolysis time-resolved microwave conductivity (FP-TRMC) measurements. C₆₀⊂H₄-CPD_{py} has an anisotropic charge mobility ($\Sigma\mu=0.16$ and $0.13\text{ cm}^2\text{ V}^{-1}\text{ s}^{-1}$) along the zigzag chain of C₆₀ (which runs at 45° and parallel to the crystallographic *b* axis). To construct a photoelectrochemical cell, C₆₀⊂H₄-CPD_{py} was deposited onto nanostructured SnO₂ films on a transparent electrode. The solar cell exhibited photovoltaic activity with an incident photon to current conversion efficiency of 17%.

[a] Dr. H. Nobukuni, Prof. Dr. Y. Naruta, Prof. Dr. F. Tani
Institute for Materials Chemistry and Engineering
Kyushu University, 6-10-1 Hakozaki
Higashi-ku, Fukuoka 812-8581 (Japan)
Fax: (+81)92-642-2715
E-mail: tanif@ms.ifoc.kyushu-u.ac.jp

[b] Prof. Dr. Y. Shimazaki
College of Science, Ibaraki University, Bunkyo
Mito 310-8512 (Japan)

[c] Prof. Dr. H. Uno
Graduate School of Science and Engineering
Ehime University, Bunkyo-cho, Matsuyama 790-8577 (Japan)


[d] Prof. Dr. K. Ohkubo, Prof. Dr. S. Fukuzumi
Department of Material and Life Science
Graduate School of Engineering, Osaka University
Suita, Osaka 565-0871 (Japan)

[e] Prof. Dr. T. Kojima
Graduate School of Pure and Applied Sciences
University of Tsukuba, Tsukuba, Ibaraki 305-8571 (Japan)

[f] Prof. Dr. S. Fukuzumi
Department of Bioinspired Science, Ewha Womans University
Seoul, 120-750 (Korea)

[g] Prof. Dr. S. Seki
Department of Applied Chemistry
Graduate School of Engineering, Osaka University
PRESTO (Japan) Science and Technology Agency (JST)
Suita, Osaka 565-0871 (Japan)

[h] Dr. H. Sakai, Prof. Dr. T. Hasobe
Department of Chemistry, Faculty of Science and Technology
Keio University
PRESTO (Japan) Science and Technology Agency (JST)
Yokohama, Kanagawa 223-8522 (Japan)

 Supporting information for this article is available on the WWW under <http://dx.doi.org/10.1002/chem.201001815>.

Introduction

Fullerene derivatives (C_{60} , C_{70} , [6,6]-phenyl C_{61} -butyric acid methyl ester (PCBM), etc) are seen as the ultimate electron acceptors because of their favorable reduction potentials and small reorganization energies in electron-transfer reactions.^[1] Hence, they are good candidate materials for molecular electronics devices.^[2] Well-ordered arrangements of fullerene derivatives in the solid state are indispensable for this application. For example, a single crystal of C_{60} has a fairly high electron mobility ($\Sigma\mu = 0.50 \text{ cm}^2 \text{ V}^{-1} \text{ s}^{-1}$) as an organic semiconductor.^[3] However, it is still difficult to rationally arrange C_{60} molecules in a deliberate manner, because C_{60} is composed of only carbon atoms, and has no functional groups. One approach is to chemically modify C_{60} by introducing functional groups.^[4] But these modifications can compromise the attractive characteristics of pristine C_{60} , because they break the symmetry and original electronic properties of C_{60} . Another solution is to use host-guest chemistry; that is, the arrangement of host molecules including C_{60} .^[5] As host molecules, electron-rich aromatic compounds, such as calixarenes, resorcinarenes, and cyclotrimeratrylenes, have generally been used in supramolecular chemistry.^[6] Porphyrin derivatives are particularly attractive components in the design of host molecules for fullerenes.^[7] Cyclic bisporphyrin hosts were first designed by Aida and Tashiro,^[8] while acyclic bisporphyrin hosts were reported by Boyd and Reed.^[9] These inclusion complexes of fullerenes with porphyrin derivatives are stable in solution and in the crystalline state due to the π - π interactions between the curved π planes of the fullerenes and the flat π planes of the porphyrins.

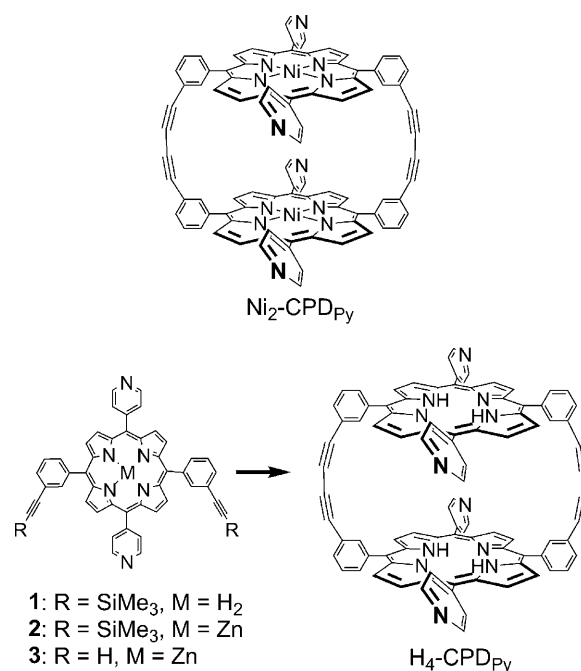
On the other hand, many porphyrin-fullerene conjugates have been extensively studied as functional models of the reaction center for charge separation in natural photosynthesis.^[10] In these conjugates, fullerenes usually behave as electron acceptors, whereas porphyrin derivatives tend to act as electron donors. Long lifetimes of charge-separated states with high quantum yields (e.g., 0.53 s and 83 %, respectively) have been reported^[11] that are comparable to those of the reaction center in natural photosynthesis. Moreover, fullerenes have been employed as n-type semiconductors, and porphyrin derivatives have been used as p-type semiconductors of the active layers in organic photovoltaic (OPV) devices.^[12] OPV devices are expected to be inexpensive, lightweight, flexible, and ubiquitous energy conversion systems in the future.^[13-15] The main advantages of OPV devices lie in their cost and processability; one can easily fabricate large-area devices, because organic materials are compatible with solution-processing techniques. But the power conversion efficiency (η) in the OPV devices reported thus far are still low. The mechanism of power conversion from light to current is composed of three important processes; light harvesting, charge separation, and carrier transport. Thus, the enhancement of the power conversion efficiency, in general, requires a highly ordered and bicontinuous donor-acceptor arrangement in the active layers because

such an arrangement represents the most effective way to achieve the three key processes.^[16]

Imahori et al. have recently reported a novel approach for constructing a vertical alignment of bicontinuous porphyrin-fullerene arrays on a flat semiconducting electrode for a photoelectrochemical device with high efficiency.^[17]

Therefore, a linear arrangement of C_{60} inside porphyrin derivative hosts is expected to provide photoinduced charge separation and smooth vectorial charge transport, both of which are the most fundamental prerequisites for efficient photovoltaics.

Recently, we reported an inclusion complex composed of a cyclic nickel porphyrin dimer (Ni_2 -CPD_{Py}, Scheme 1) and C_{60} .^[18] In this complex ($C_{60} \subset Ni_2$ -CPD_{Py}), C_{60} molecules are



Scheme 1. Molecular structure of Ni_2 -CPD_{Py} and synthetic route for H_4 -CPD_{Py}.

linearly arranged in the inner channel of the porphyrin nanotube to form a supramolecular peapod. In addition, the complex exhibits a high anisotropic electron mobility ($\Sigma\mu = 0.72 \text{ cm}^2 \text{ V}^{-1} \text{ s}^{-1}$) along the linear arrangement of C_{60} .^[19] However, the expected charge-separated state was not observed in the time-resolved transient absorption spectra of $C_{60} \subset Ni_2$ -CPD_{Py} because the singlet excited state of the nickel porphyrin immediately gives rise to the triplet excited state by intersystem crossing,^[20] and the low-energy triplet excited state of C_{60} (${}^3C_{60}^*$) is then formed by energy transfer.^[21] The estimated energy level of the charge-separated state (1.98 eV) is higher than that of ${}^3C_{60}^*$ (1.60 eV).^[22] Thus, the corresponding free-base porphyrin compound is more likely to yield a charge-separated state for the following reasons: 1) a free-base porphyrin generally has a lower oxidation potential than that of the corresponding nickel

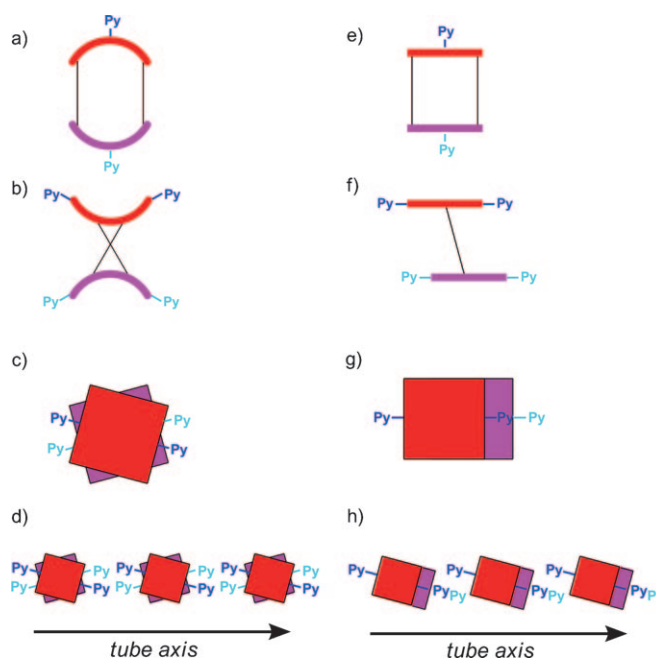
complex, so the desired charge separation becomes more feasible; and 2) an intersystem crossing from a singlet excited state to a triplet excited state for a free-base porphyrin would be much slower than that of the corresponding nickel complex. Herein, we report the supramolecular structures and photoelectrochemical properties of the inclusion complex of the free-base porphyrin dimer (H₄-CPD_{Py}, Scheme 1) and C₆₀. The structure of this complex (C₆₀⊂H₄-CPD_{Py}) was characterized by X-ray crystallography. We investigated the photodynamics of C₆₀⊂H₄-CPD_{Py} in the solid state by femto-second laser flash photolysis. The charge-carrier mobility of C₆₀⊂H₄-CPD_{Py} in the single crystal was determined by flash-photolysis time-resolved microwave conductivity (FP-TRMC) measurements.^[23] Furthermore, the photovoltaic properties of C₆₀⊂H₄-CPD_{Py} were also studied and compared with those of C₆₀⊂Ni₂-CPD_{Py}.

Results and Discussion

Formation and structure of a porphyrin nanotube: H₄-CPD_{Py} was synthesized from the corresponding zinc porphyrin monomer with two terminal C≡C triple bonds by Glaser coupling catalyzed by copper(I) under air in 20% yield (Scheme 1). The zinc monomer rather than the free-base monomer was used to inhibit copper ion insertion to the porphyrin.^[24] The zinc ion was easily removed by acid treatment.

Purple crystals of H₄-CPD_{Py} suitable for X-ray crystallography were grown by slow evaporation of a solution in CHCl₃/*o*-dichlorobenzene. The H₄-CPD_{Py} molecule has a rectangular shape (Figure 1 a–c).^[25] The distances between the centers of the two porphyrin rings and the two mid-points of the butadiyne moieties are 10.785 and 14.247 Å,

respectively. In comparison with the structure of the Ni₂-CPD_{Py} molecule,^[18] the H₄-CPD_{Py} molecule has two characteristic features (Scheme 2): 1) The porphyrin rings show a higher planarity. The displacements of the *meso* carbon atoms from the four-nitrogen mean plane (−0.154, −0.055, −0.216, 0.145 Å, positive values meaning outward) are much smaller than those of Ni₂-CPD_{Py} (−0.473, 0.553, −0.603, 0.503 Å), and 2) the two porphyrin rings are in a “slipped”



Scheme 2. Schematic representations of structural features in the single crystals of a)–d) Ni₂-CPD_{Py} and e)–h) H₄-CPD_{Py}. a), e) front view; b), f) side view; c), g) top view; d), h) tubular assembly.

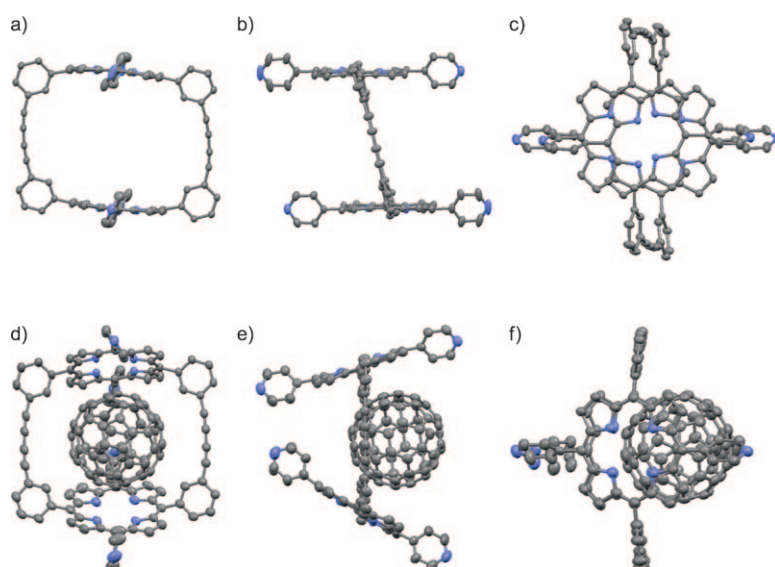


Figure 1. ORTEP drawings of a)–c) H₄-CPD_{Py} and d)–f) C₆₀⊂H₄-CPD_{Py} with 50% probability thermal ellipsoids (solvent molecules and hydrogen atoms are omitted for clarity). a), d) front view; b), e) side view; c), f) top view.

arrangement with respect to each other, and are not rotated around the center-to-center axis from the top view (Figure 1 c). Also, the two butadiyne moieties are coplanar from the side view (Figure 1 b). Seven *o*-dichlorobenzene molecules of crystallization per H₄-CPD_{Py} molecule are incorporated into the structure; five inside the cavity, and two outside, but they are severely disordered.

A novel porphyrin nanotube can be observed in the crystal packing of H₄-CPD_{Py} (Figure 2 and Figure S1 in the Supporting Information).^[26] The tubular structure is formed along the direction of the crystallographic *a* axis by self-assembly through

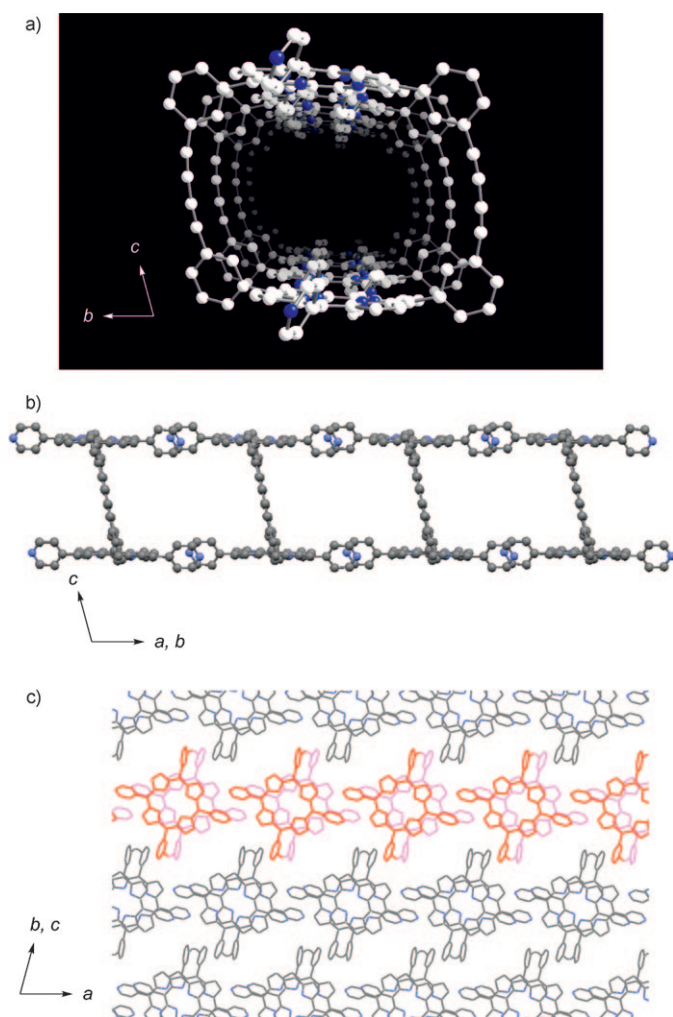


Figure 2. Crystal structures of tubular assemblies of H_4 -CPD $_{py}$. *o*-Dichlorobenzene molecules and hydrogen atoms are omitted for clarity. a) front view; b) side view; c) top view. In a) and b), N = blue; C = gray.

two kinds of cooperative noncovalent interaction between the cyclic molecules (Figure 3). One is a pair of complementary C–H...N hydrogen-bonding interactions between the pyrrole β -CH and the nitrogen atoms of the pyridyl groups,

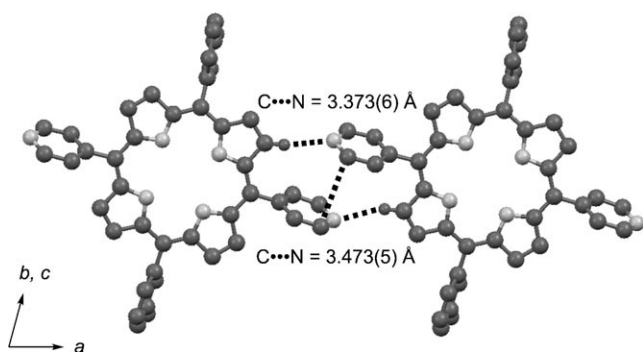


Figure 3. Details of the noncovalent interactions linking the cyclic porphyrin dimers in the crystal of H_4 -CPD $_{py}$. Hydrogen atoms are omitted except in the C–H...N moieties. N = gray; C, H = black.

with C...N distances of 3.373(6) and 3.473(5) Å. The other noncovalent interaction is a weak π – π interaction between the pyridyl groups. For this interaction, the shortest carbon–carbon distance is 3.645(8) Å, and the dihedral angle is 7.45°. In total, the adjacent dimers along the *a* axis are linked by four hydrogen bonds and two π – π interactions. These interactions are similar to those of the crystal structure of Ni_2 -CPD $_{py}$.^[18] The center-to-center distance between porphyrins along this tubular assembly is 14.895 Å for H_4 -CPD $_{py}$. In both Ni_2 -CPD $_{py}$ and H_4 -CPD $_{py}$, each tube axis is not parallel with the vector joining the pyridyl-substituted *meso* carbon atoms; that is, each vector has a certain oblique angle to each tube axis. However, there is a clear difference between the arrangements of the porphyrin moieties in Ni_2 -CPD $_{py}$ and H_4 -CPD $_{py}$ (Scheme 2). In the Ni_2 -CPD $_{py}$ tubes, the two vectors of the upper and lower porphyrins show opposite oblique angles relative to the tube axis. On the other hand, the vectors of the two porphyrins of H_4 -CPD $_{py}$ exhibit the same oblique angle relative to the tube axis.

Inclusion properties of C_{60} with H_4 -CPD $_{py}$ in solution: As expected from the distance between the centers of the two porphyrin rings (10.785 Å), which is comparable to the outer diameter of C_{60} (about 10.3 Å), H_4 -CPD $_{py}$ can include C_{60} inside its cavity in solution. The UV/Vis absorption spectral change during the addition of C_{60} to the solution of H_4 -CPD $_{py}$ in $CHCl_3$ /toluene (1:1) is shown in Figure 4. The Soret band was redshifted with a decrease in intensity, whereas the Q band was also redshifted but increased in intensity. The Job plot (415 nm) upon mixing H_4 -CPD $_{py}$ and C_{60} also displayed a signature pattern for the formation of a 1:1 host–guest complex ($C_{60} \subset H_4$ -CPD $_{py}$) (see Figure S2 in the Supporting Information).^[26] On the basis of the titration of H_4 -CPD $_{py}$ with C_{60} , the association constant (K_{assoc}) was determined to be $9.6 \times 10^4 M^{-1}$ (Figure S3 in the Supporting Information).^[26] This value is nearly half that of Ni_2 -CPD $_{py}$ ^[18] and is smaller than that of the cyclic free-base porphyrin dimer ($7.5 \times 10^5 M^{-1}$) linked by $-O(CH_2)_6O-$ spacers rather than by butadiyne.^[27]

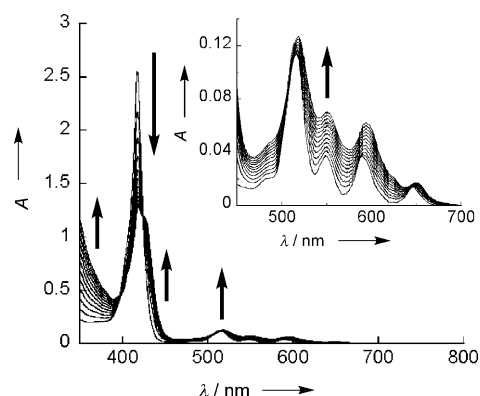


Figure 4. Absorption spectral changes of H_4 -CPD $_{py}$ upon titration with C_{60} in $CHCl_3$ /toluene (1:1) at room temperature. The inset shows the Q-band region. $[H_4$ -CPD $_{py}] = 4.0 \times 10^{-6} M$, $[C_{60}] = 3.9 \times 10^{-6}$ – $3.6 \times 10^{-5} M$.

ESIMS of a 1:1 mixture of H₄-CPD_{Py} and C₆₀ in CH₂Cl₂/methanol/CH₃COOH (50:50:0.2) revealed two peak clusters at *m/z* 2047.3 ([H₄-CPD_{Py}+C₆₀]⁺) and 1023.7 ([H₄-CPD_{Py}+C₆₀]²⁺) with no peaks of free H₄-CPD_{Py} and C₆₀ (Figure S4 in the Supporting Information).^[26] These spectra indicate that the 1:1 complex of H₄-CPD_{Py} with C₆₀ is stable. The ¹³C NMR spectrum of a 1:1 mixture of H₄-CPD_{Py} and ¹³C-enriched C₆₀ in CDCl₃/[D₈]toluene (1:1) showed a singlet signal arising from included C₆₀ at δ = 141.1 ppm, which is shifted upfield from that of free C₆₀ (δ = 143.4 ppm) on account of the ring-current effect of the porphyrins (Figure S5 in the Supporting Information).^[26]

The redox potentials of H₄-CPD_{Py}, C₆₀ and C₆₀⊂H₄-CPD_{Py} were determined by voltammetry (Table 1) (Figure S6 in the Supporting Information).^[26] In the thin-film state on the

Table 1. Redox potentials (versus Fc⁺/Fc) of H₄-CPD_{Py}, C₆₀, and C₆₀⊂H₄-CPD_{Py} with 0.1 M *n*Bu₄NClO₄.

Compound	Oxidation ^[a] <i>E</i> ₁ ^p	Reduction ^[b] <i>E</i> ₁ ^{1/2}
H ₄ -CPD _{Py}	0.81	–
C ₆₀	–	–0.97
C ₆₀ ⊂H ₄ -CPD _{Py}	0.83	–1.00

[a] The oxidation potentials were analyzed by DPV of film states of the samples on platinum electrodes in acetonitrile with 0.1 M *n*Bu₄NClO₄. [b] The reduction potentials were determined by cyclic voltammetry in *o*-dichlorobenzene/pyridine (1:1) with 0.1 M *n*Bu₄NClO₄. Scan rate = 0.1 V s^{–1}. The concentration was 0.2 mM.

electrode, the oxidation potential of the porphyrin unit in C₆₀⊂H₄-CPD_{Py} (0.83 V versus Fc⁺/Fc by differential pulse voltammetry (DPV)) showed a 0.02 V anodic shift compared with that of H₄-CPD_{Py} (0.81 V). In comparison with that of Ni₂-CPD_{Py} (0.88 V), these potentials are slightly lower. In cyclic voltammograms of *o*-dichlorobenzene/pyridine (1:1), the first cathodic process corresponding to the reduction of the fullerene entity of C₆₀⊂H₄-CPD_{Py} was observed at –1.00 V, which is cathodically shifted by 0.03 V in comparison with pristine C₆₀ (–0.97 V). The small anodic shift of the oxidation potential of the porphyrin and the small cathodic shift of the reduction potential of C₆₀ compared with their reference compounds are indicative of the charge-transfer interaction between the porphyrins and C₆₀.^[8, 19, 28–30]

Crystal structure of the inclusion complex of C₆₀ with H₄-CPD_{Py}:

Black single crystals of C₆₀⊂H₄-CPD_{Py} were prepared from a 1:1 mixture of H₄-CPD_{Py} in CHCl₃ and C₆₀ in toluene. X-ray crystallography revealed a 1:1 inclusion complex of C₆₀ with H₄-CPD_{Py} (Figure 1d–f).^[25] In the crystal structure of C₆₀⊂H₄-CPD_{Py}, the dimer includes a C₆₀ molecule in a clamshell-like conformation, in which the porphyrin rings are tilted with respect to each other. The dihedral angle of the two porphyrin planes is 52.38°, which is in stark contrast to the parallel conformation in the crystal structure of H₄-CPD_{Py}. The increase of the distance (11.126 Å) between the centers of the two porphyrins and the decrease of that (13.915 Å) between the midpoints of the butadiene

moieties are also observed upon inclusion. On the other hand, the porphyrin rings maintain planarity; the displacements of the *meso* carbon atoms from the four-nitrogen mean plane are –0.299, 0.190, –0.256, –0.106, –0.246, –0.042, –0.151, –0.161 Å (positive values meaning outward). These results indicate that inclusion induces a drastic structural change, presumably because the distance between the two porphyrins is too short to accommodate C₆₀ in the parallel conformation. Although Ni₂-CPD_{Py} has the same butadienyl spacer groups, the porphyrin was saddle-distorted to give a longer center-to-center distance (12.596 Å for C₆₀⊂Ni₂-CPD_{Py}), and to accommodate C₆₀ in the parallel conformation. In most examples of inclusion complexes of C₆₀ with porphyrins, a 6:6 ring-juncture C–C bond of the fullerene is closest to the porphyrin.^[7, 8] In the present case, however, the nearest bond of C₆₀ is the 6:5 juncture. The shortest separations between the carbon atoms of C₆₀ and the porphyrin centers are 2.850, 2.903, 3.025 and 3.065 Å (Figure 5). These values represent fairly strong π–π interactions between the porphyrins and C₆₀. There is one water molecule and at least three toluene molecules per H₄-CPD_{Py} molecule in the structure. Elemental analysis supports this composition. The toluene molecules are highly disordered, and are taken into account by the PLATON Squeeze technique.^[31]

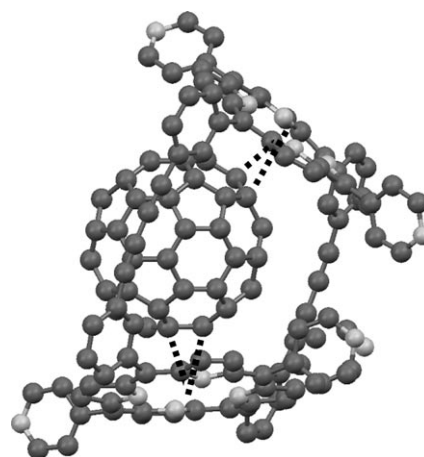


Figure 5. Details of the noncovalent interactions between H₄-CPD_{Py} and C₆₀. Hydrogen atoms are omitted. N = gray; C = black.

In contrast, C₆₀⊂H₄-CPD_{Py} shows a highly symmetric ¹H NMR spectrum in solution at room temperature. The included C₆₀ molecule would oscillate in the cavity much faster than the NMR timescale and/or would be positioned above the center of the porphyrin ring in solution.

To our surprise, the C₆₀ molecules form a zigzag chain along the crystallographic *b* axis in the crystal packing, and a nanotube structure is no longer observed (Figure 6). The distance between the centers of the adjacent C₆₀ molecules along the zigzag array (arrow A in Figure 6a) is 10.018 Å. This value is comparable to the outer diameter of C₆₀ (ca. 10.3 Å). In other words, the C₆₀ molecules have van der

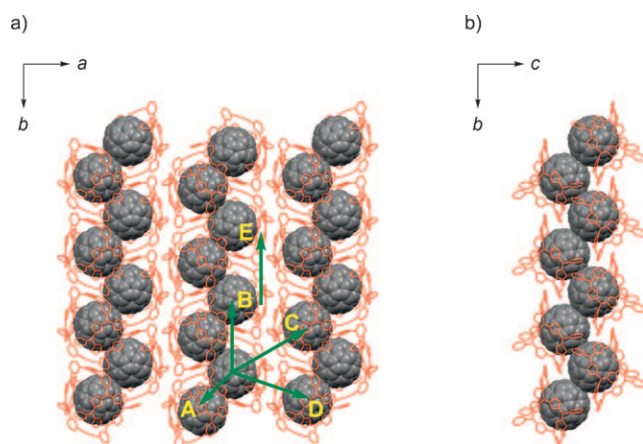


Figure 6. Zigzag arrays of $C_{60}CH_4$ -CPD_{py} in the crystal structures. Solvent molecules and hydrogen atoms are omitted for clarity. The H_4 -CPD_{py} units and the C_{60} molecules are depicted by wire frames and space-filling models, respectively. a) Top view; b) side view.

Waals contacts with each other along the zigzag arrangement. This zigzag array is derived from a partial covering of H_4 -CPD_{py}. The uncovered π plane of the three-dimensional and symmetrical C_{60} molecule (rather than two-dimensional common aromatic compounds) enables these interesting interactions. The distances between the centers of the C_{60} molecules along the parallel direction to b axis (arrow B) and in the adjacent zigzag arrays (arrows C and D) are 15.059, 18.161, and 16.250 Å, respectively. The two distances marked by arrows B and E are equivalent. The two porphyrin rings facing each other along the a axis are very close, with the shortest nitrogen–nitrogen distance 3.462 Å.

Photochemical properties of the inclusion complex of C_{60} with H_4 -CPD_{py}: Time-resolved transient absorption spectra in the solid state for H_4 -CPD_{py} and $C_{60}CH_4$ -CPD_{py} in KBr pellets were obtained by femtosecond laser flash photolysis after photoexcitation at 420 nm (Figure 7). A sharp peak at 1070 nm assignable to the radical anion of C_{60} ($C_{60}^{\cdot-}$)^[32] was observed in the transient absorption spectra of $C_{60}CH_4$ -CPD_{py}. This clearly differs from the results of $C_{60}Ni_2$ -CPD_{py}. Thus, the formation of a completely charge-separated state $\{H_4\text{-CPD}_{py}^{\cdot+} + C_{60}^{\cdot-}\}$ was confirmed, although the absorbance due to the radical cation of the porphyrin ($H_4\text{-CPD}_{py}^{\cdot+}$) in the 500–800 nm region is not clear because there would be overlap with the bleaching of the porphyrin Q-band absorption. The electron transfer from the porphyrin singlet excited state to C_{60} is also supported by the quenching of the porphyrin fluorescence from 650 to 750 nm in the spectrum of $C_{60}CH_4$ -CPD_{py} in comparison with that of H_4 -CPD_{py} (Figure S7 in the Supporting Information). The fluorescence of the free-base porphyrin is observed in this region as a valley in the spectra of H_4 -CPD_{py} (Figure 7a). The decay of the absorption band at 1070 nm of $C_{60}CH_4$ -CPD_{py} has two steps, as shown in Figure 8. The first step has a lifetime of 18 ps, which corresponds to the disappearance of the singlet excited state of the porphyrin $^1H_4\text{-CPD}_{py}^*$.

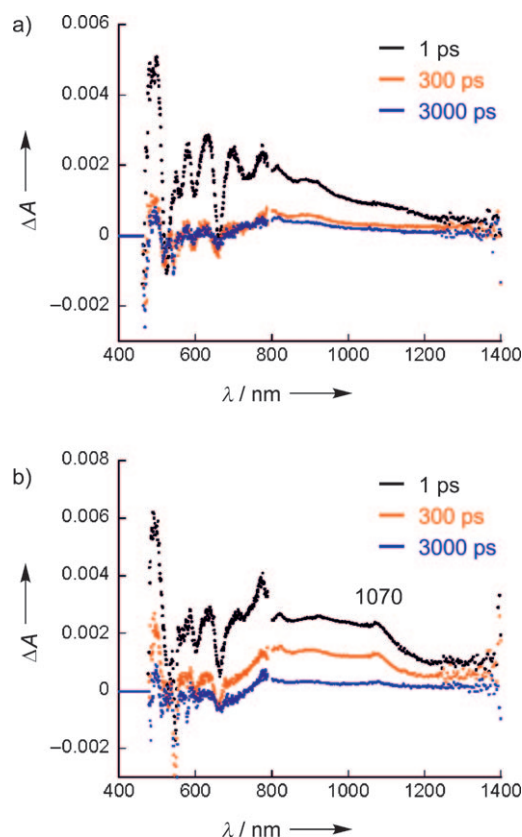


Figure 7. Transient absorption spectra of a) H_4 -CPD_{py} and b) $C_{60}CH_4$ -CPD_{py} recorded at 1, 300, and 3000 ps after photoexcitation at 420 nm in KBr pellets.

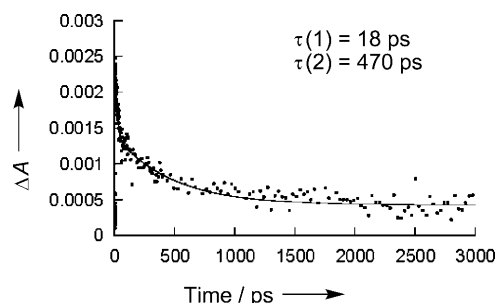


Figure 8. Decay-time profile of the absorption of $C_{60}CH_4$ -CPD_{py} in a KBr pellet at 1070 nm.

The S_1 of the porphyrin has a broad absorption from 800 to 1200 nm, as shown in Figure 7a. The second component coincides with the decay of $\{H_4\text{-CPD}_{py}^{\cdot+} + C_{60}^{\cdot-}\}$, which has a lifetime of 470 ps.

The photodynamics in the solid of $C_{60}CH_4$ -CPD_{py} is summarized in Figure 9. Photoexcitation at 420 nm immediately affords both the singlet excited state of porphyrin $^1H_4\text{-CPD}_{py}^*$ (1.90 eV)^[33] and the singlet excited state of fullerene $^1C_{60}^*$ (2.00 eV).^[34] Both species undergo intrasupramolecular electron transfer to give a charge-separated state $\{H_4\text{-CPD}_{py}^{\cdot+} + C_{60}^{\cdot-}\}$ (1.83 eV), the energy level of which can be estimated from the difference between the one-electron re-

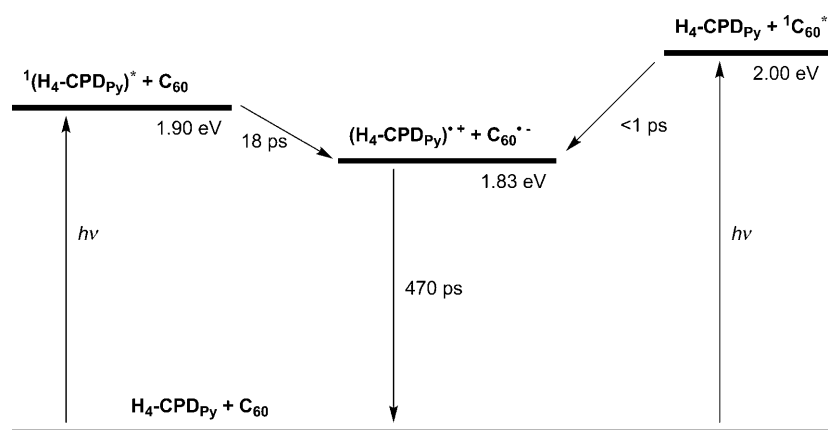


Figure 9. Energy diagram for the photochemical events in C₆₀C(H₄-CPD)_{Py}.

duction potential of C₆₀ and the oxidation potential of the porphyrin moieties in C₆₀C(H₄-CPD)_{Py} (Table 1). However, electron-transfer rates in the two pathways are different; 18 ps in ¹H₄-CPD)_{Py}^{*}, whereas ¹C₆₀^{*} decays within 1 ps. Meanwhile, the charge-separated state has a lifetime of 470 ps, and it decays directly to the ground state.

A charge-separated state was clearly detected for C₆₀C(H₄-CPD)_{Py}, but not for C₆₀C(Ni₂-CPD)_{Py}.^[19] This is probably because the energy level of the charge-separated state of C₆₀C(H₄-CPD)_{Py} (1.83 eV) is lower than that of C₆₀C(Ni₂-CPD)_{Py} (1.98 eV). Also, the free-base porphyrin has a much slower intersystem crossing to its triplet excited state, which would undergo energy transfer to C₆₀. This would result in the lower-energy C₆₀ triplet excited state instead of the charge-separated state. Thus, it is possible to improve the efficiency of the charge separation by tuning the electronic properties of the porphyrin moiety.

Charge mobility of the inclusion complex of C₆₀ with H₄-CPD)_{Py}: The zigzag array of C₆₀ molecules, formed through van der Waals contacts with each other, and the clear formation of the radical anion of C₆₀ (C₆₀^{•-}) are expected to lead to high electron mobility in the C₆₀C(H₄-CPD)_{Py} crystal. To measure the charge mobility in C₆₀C(Ni₂-CPD)_{Py}, a single crystal was subjected to FP-TRMC measurements.^[23] The TRMC technique holds several advantages over time of flight (TOF) and field-effect transistor (FET) methods: 1) there is no need for electrodes, 2) analysis of the anisotropic charge transport can be made in the single crystal, 3) detection of charge carrier mobility can be made on the nanometer scale, and 4) small effects arising through chemical or physical defects of the crystals can be detected.

We have determined the face indices of C₆₀C(H₄-CPD)_{Py} by X-ray crystallographic analysis (Figure 10). The crystal exhibits a platelike shape. The zigzag chain of C₆₀ runs down the longest axis of the crystal. The electric field of the resonant microwave in the cavity was applied at various directions relative to the crystallographic *b* axis to investigate the anisotropy of the charge mobility.

The transient conductivity in the single crystal of C₆₀C(H₄-CPD)_{Py} was measured by using TRMC (Figure 11 shows the kinetic traces). The transient conductivity can be expressed as ($\phi\Sigma\mu$), in which ϕ and $\Sigma\mu$ denote photocarrier generation yield (quantum efficiency) and the sum of mobilities for negative and positive carriers, respectively. Upon irradiation with a laser pulse of excitation wavelength of 532 nm, the single crystal of C₆₀C(H₄-CPD)_{Py}

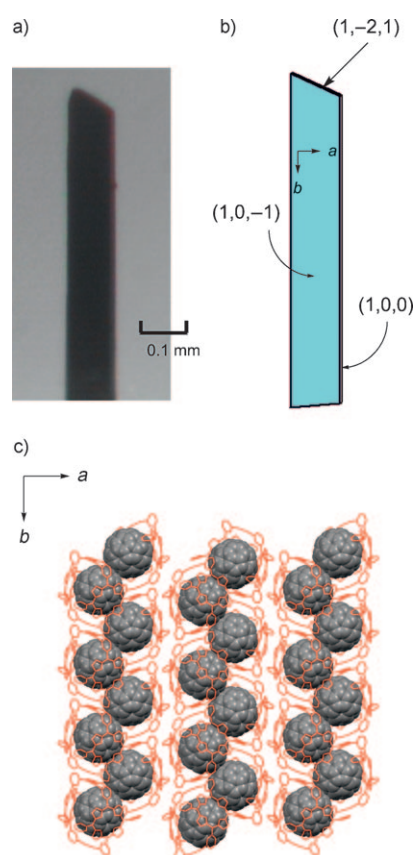


Figure 10. A view of the single crystal of C₆₀C(H₄-CPD)_{Py} and the face indices determined by X-ray crystallographic analysis. a) Photograph of the crystal of C₆₀C(H₄-CPD)_{Py}. b) Crystal shape with the indices for C₆₀C(H₄-CPD)_{Py}. c) Molecular arrangement of C₆₀C(H₄-CPD)_{Py} corresponding to the photograph.

revealed a strong transient conductivity $\phi\Sigma\mu$ with peaks of $5.2 \times 10^{-3} \text{ cm}^2 \text{ V}^{-1} \text{ s}^{-1}$ at 45° to the *b* axis, $4.1 \times 10^{-3} \text{ cm}^2 \text{ V}^{-1} \text{ s}^{-1}$ along the *b* axis, and $9.8 \times 10^{-4} \text{ cm}^2 \text{ V}^{-1} \text{ s}^{-1}$ at 90° to the *b* axis.

To determine the value of the charge-carrier mobility $\Sigma\mu$, the ϕ value was obtained by the conventional direct-current

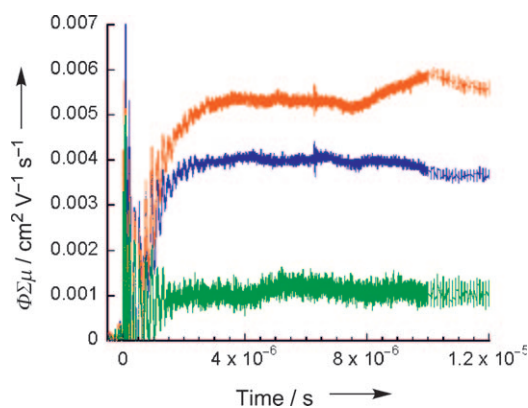


Figure 11. Conductivity transients for the single crystal of $C_{60}C_4H_4-CPD_{Py}$. The red, blue, and green curves correspond to the conductivity at 45°, parallel, and 90° to the b axis, respectively.

current integration (DC-CI) method, in which thin films of $C_{60}C_4H_4-CPD_{Py}$ were spin-coated from a solution of $C_{60}C_4H_4-CPD_{Py}$ in $CHCl_3$ /toluene (1:1) on a brush-shaped electrode with a 5 μm gap under excitation at 532 nm with a power density ranging from 4.8 to 7.2 $mJ cm^{-2}$.^[26] The maximum yield of photocarrier generation obtained under an applied bias was $\phi = 0.032$. Note that the current transients were obtained under an applied bias with a range of 2.0×10^3 to $6.4 \times 10^4 V cm^{-1}$ between the electrodes. To identify the charge carrier (electron or hole) we also made measurements by using thin films of $C_{60}C_4H_4-CPD_{Py}$ sandwiched between Al and semitransparent Au electrodes. The transient current was observed under both negative and positive biases of ± 0.5 – $3.1 \times 10^5 V cm^{-1}$ with an illumination of 16 $mJ cm^{-2}$. This indicates that both electron and hole act as charge carriers in $C_{60}C_4H_4-CPD_{Py}$. The current integration of electron (25 $\mu C cm^{-2}$) is 20 times that of hole (1.2 $\mu C cm^{-2}$). Hence, the main charge carrier is the electron transported by the C_{60} molecules. Assuming that the ϕ values in the single crystal are the same as those in the film, the single crystal of $C_{60}C_4H_4-CPD_{Py}$ exhibits minimum charge mobilities of 0.16, 0.13, and 0.030 $cm^2 V^{-1} s^{-1}$ at 45°, parallel, and 90° to the b axis, respectively.^[35]

The observed highest value (0.16 $cm^2 V^{-1} s^{-1}$) for $C_{60}C_4H_4-CPD_{Py}$ is lower than that of $C_{60}C_{Ni_2}-CPD_{Py}$ (0.72 $cm^2 V^{-1} s^{-1}$), in spite of the C_{60} – C_{60} van der Waals contacts in $C_{60}C_4H_4-CPD_{Py}$. This is probably because the C_{60} molecules are in a zigzag arrangement rather than in a straight line. The pairs of C_{60} molecules are not continuous along the 45° direction to the b axis (arrow A in Figure 6a); that is, one pair is separated from the other pairs along this direction. Electron transport between the pairs of the adjacent zigzag arrays seems to be retarded due to the distance (18.161 Å) between them (see arrow C in Figure 6a) and the presence of the intervening groups such as the phenyl groups. Effective electron transport would only occur in the range of around 2 nm (the sum of the outer diameter of two C_{60} molecules), although TRMC measurements suggest charge carrier mobility on the scale of a few nanometers.^[23]

In contrast, the higher electron mobility of $C_{60}C_{Ni_2}-CPD_{Py}$ was ascribed to the continuous linear array of C_{60} molecules with no intervening groups. The anisotropic mobility along the b axis (0.13 $cm^2 V^{-1} s^{-1}$) is comparable to that along the 45° direction, although the distance between the center of C_{60} molecules along the b axis (15.059 Å, arrow B) is longer than between those (10.018 Å) at 45° to the b axis. This may result from the continuous arrangement of the C_{60} molecules along the b axis with the intervening butadiynyl groups, the steric hindrance of which is relatively small. Moreover, the porphyrins along the b axis would also contribute to the charge (hole) transport (arrow E). On the other hand, the mobility (0.030 $cm^2 V^{-1} s^{-1}$) along the direction vertical to the b axis (arrow D) is much smaller, because the donor–acceptor (porphyrin– C_{60}) alternating array is formed in this direction. As a whole, these results show that charge transport, mainly electron transport, along the well-ordered zigzag array (at 45° and parallel to the b axis) is more feasible than along the other directions.

Photoelectrochemistry of the inclusion complexes of C_{60} with H_4-CPD_{Py} : Efficiencies of formation of the charge-separated state and carrier transport are key factors in the photovoltaic process. To evaluate the solar-energy conversion properties, photoelectrochemical cells composed of $C_{60}C_4H_4-CPD_{Py}$ or $C_{60}C_{Ni_2}-CPD_{Py}$ were fabricated. Figure 12 shows

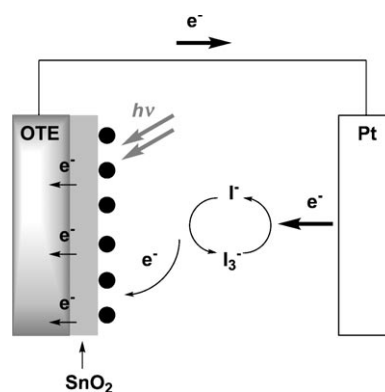


Figure 12. Illustration of the photoelectrochemical cell.

an illustration of the photocurrent measurement system of an optically transparent electrode (OTE) with an I^-/I_3^- redox couple as an electrolyte system.^[12f-h] For this measurement, clusters of $C_{60}C_4H_4-CPD_{Py}$ and $C_{60}C_{Ni_2}-CPD_{Py}$ were prepared by using the following procedure: First, the 1:1 mixture of H_4-CPD_{Py} or Ni_2-CPD_{Py} in $CHCl_3$ (1 mM) and C_{60} in o -dichlorobenzene (1 mM) was prepared. Then, the mixture (1 mL) was diluted with hexane (3 mL; final concentration: 125 μM in $CHCl_3/o$ -dichlorobenzene/hexane = 1:1:6, denoted as $(C_{60}C_4H_4-CPD_{Py})_n$ and $(C_{60}C_{Ni_2}-CPD_{Py})_n$). The “reference” clusters H_4-CPD_{Py} , Ni_2-CPD_{Py} , and C_{60} were also prepared (denoted as $(H_4-CPD_{Py})_n$, $(Ni_2-CPD_{Py})_n$, and $(C_{60})_n$, respectively). Figure 13 shows the TEM images of all clusters. Interestingly, clusters with diameters of the order of

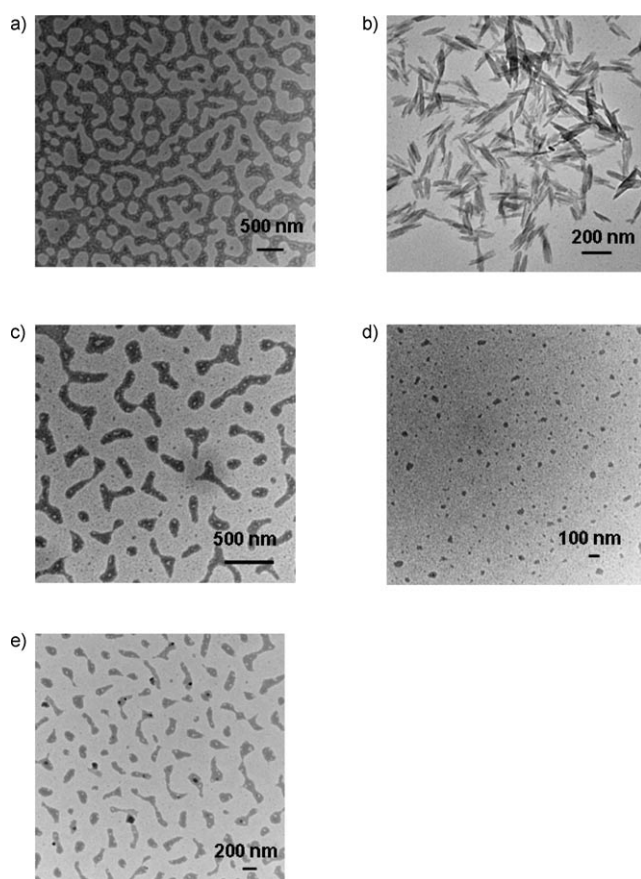


Figure 13. TEM images of a) $(C_{60}C_4\text{-CPD}_{\text{py}})_n$, b) $(H_4\text{-CPD}_{\text{py}})_n$, c) $(C_{60}CNi_2\text{-CPD}_{\text{py}})_n$, d) $(Ni_2\text{-CPD}_{\text{py}})_n$, and e) $(C_{60})_n$.

hundreds of nm were formed in the cases of $(C_{60}C_4\text{-CPD}_{\text{py}})_n$, $(H_4\text{-CPD}_{\text{py}})_n$, $(C_{60}CNi_2\text{-CPD}_{\text{py}})_n$, and $(C_{60})_n$, but not in the case of $(Ni_2\text{-CPD}_{\text{py}})_n$. $(C_{60}C_4\text{-CPD}_{\text{py}})_n$ gave rise to especially large clusters; even greater than the sum of the sizes of $(H_4\text{-CPD}_{\text{py}})_n$ and $(C_{60})_n$. In contrast, the clusters of $(C_{60}CNi_2\text{-CPD}_{\text{py}})_n$ were similar to the summation of $(Ni_2\text{-CPD}_{\text{py}})_n$ and $(C_{60})_n$. Dynamic light scattering (DLS) measurements support the TEM results. Figure S9 in the Supporting Information shows the DLS results of $(C_{60}C_4\text{-CPD}_{\text{py}})_n$, $(H_4\text{-CPD}_{\text{py}})_n$, $(C_{60}CNi_2\text{-CPD}_{\text{py}})_n$, $(Ni_2\text{-CPD}_{\text{py}})_n$, and $(C_{60})_n$ prepared under the same conditions. The average diameter of $(C_{60}C_4\text{-CPD}_{\text{py}})_n$ (1300 nm) was larger than that of $(H_4\text{-CPD}_{\text{py}})_n$ (220 nm), $(C_{60}CNi_2\text{-CPD}_{\text{py}})_n$ (530 nm), or $(C_{60})_n$ (190 nm). On the other hand, the average diameter of $(Ni_2\text{-CPD}_{\text{py}})_n$ (44 nm) was small. The absorption spectra of these composite clusters also show the broadened aggregated features (Figure S10 in the Supporting Information).

The clusters composed of $C_{60}C_4\text{-CPD}_{\text{py}}$ and $C_{60}CNi_2\text{-CPD}_{\text{py}}$ were assembled on a nanostructured SnO_2 electrode (denoted as OTE/ SnO_2). An electrophoretic deposition procedure was applied to deposit these clusters from a CHCl_3 /*o*-dichlorobenzene/hexane suspension. Upon application of a DC electric field of 200 V cm^{-1} for 1 min between the OTE/ SnO_2 and OTE electrodes, which were kept parallel in a CHCl_3 /*o*-dichlorobenzene/hexane suspension containing

$C_{60}C_4\text{-CPD}_{\text{py}}$ and $C_{60}CNi_2\text{-CPD}_{\text{py}}$, the clusters were deposited on the SnO_2 nanocrystallites (denoted as OTE/ SnO_2 / $(C_{60}C_4\text{-CPD}_{\text{py}})_n$ and OTE/ SnO_2 / $(C_{60}CNi_2\text{-CPD}_{\text{py}})_n$, respectively). Figure 14 shows the absorption spectra of OTE/ SnO_2 / $H_4\text{-CPD}_{\text{py}}$ and OTE/ SnO_2 / $Ni_2\text{-CPD}_{\text{py}}$ on OTE films after deposition, which largely agrees with those of $(C_{60}C_4\text{-CPD}_{\text{py}})_n$ and $(C_{60}CNi_2\text{-CPD}_{\text{py}})_n$ (Figure S10 in the Supporting Information). This suggests that an interpenetrating structure is formed from $(C_{60}C_4\text{-CPD}_{\text{py}})_n$ and $(C_{60}CNi_2\text{-CPD}_{\text{py}})_n$ on OTE/ SnO_2 .

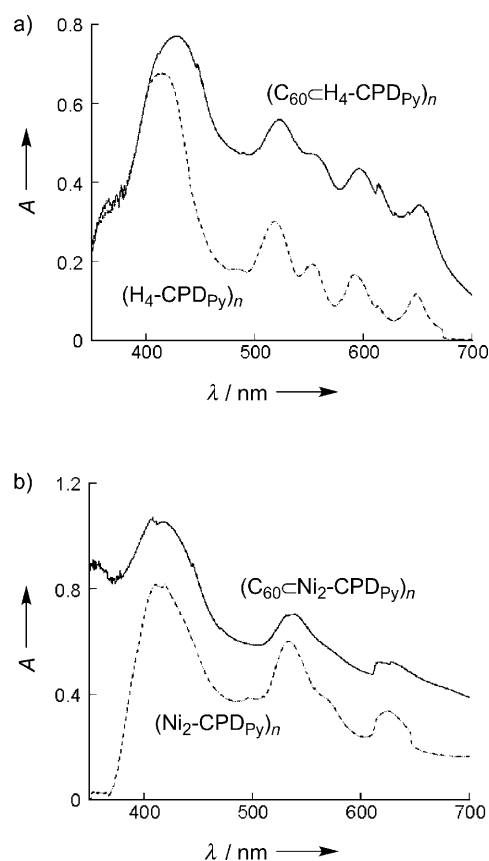


Figure 14. Absorption spectra of a) OTE/ SnO_2 / $(C_{60}C_4\text{-CPD}_{\text{py}})_n$ (solid line) and OTE/ SnO_2 / $(H_4\text{-CPD}_{\text{py}})_n$ (dotted line), and b) OTE/ SnO_2 / $(C_{60}CNi_2\text{-CPD}_{\text{py}})_n$ (solid line) and OTE/ SnO_2 / $(Ni_2\text{-CPD}_{\text{py}})_n$ (dotted line).

To evaluate the photoelectrochemical performance of the $(C_{60}C_4\text{-CPD}_{\text{py}})_n$ and $(C_{60}CNi_2\text{-CPD}_{\text{py}})_n$ films, we used the OTE/ SnO_2 as a photoanode in a photoelectrochemical cell. Photocurrent measurements were performed in acetonitrile containing LiI (0.5 M) and I_2 (0.05 M) as a redox electrolyte with a Pt gauge counter electrode.^[12] The photocurrent and photovoltage responses following the excitation of the OTE/ SnO_2 / $(C_{60}C_4\text{-CPD}_{\text{py}})_n$ and OTE/ SnO_2 / $(C_{60}CNi_2\text{-CPD}_{\text{py}})_n$ electrodes in the visible-light region (AM (air mass) = 1.5) are shown in Figure S11 in the Supporting Information. The photocurrent response is prompt, steady, and reproducible during repeated on/off cycles of visible-light illumination. The short-circuit photocurrent density (I_{sc}) of 1.10 mA cm^{-2}

and open-circuit voltage (V_{oc}) of 300 mV were reproducibly obtained during these measurements. These experiments confirmed the potential of $(C_{60}\text{C}H_4\text{-CPD}_{Py})_n$ and $(C_{60}\text{C}Ni_2\text{-CPD}_{Py})_n$ for harvesting light energy and generating photocurrent during the operation of a photoelectrochemical cell.

To evaluate the spectral photoresponses of $(C_{60}\text{C}H_4\text{-CPD}_{Py})_n$, $(C_{60}\text{C}Ni_2\text{-CPD}_{Py})_n$, $(H_4\text{-CPD}_{Py})_n$, and $(Ni_2\text{-CPD}_{Py})_n$ on OTE/SnO₂, photocurrent action spectra were also measured by using a standard two-electrode system in photoelectrochemical cells (Figure 15).^[12f-h] The incident photon to current efficiency (IPCE) values were calculated by normalizing the photocurrent values for the incident-light energy and intensity in Equation (1).^[12j]

$$\text{IPCE (\%)} = 100 \times 1240 \times I_{sc} / (W_{in} \times \lambda) \quad (1)$$

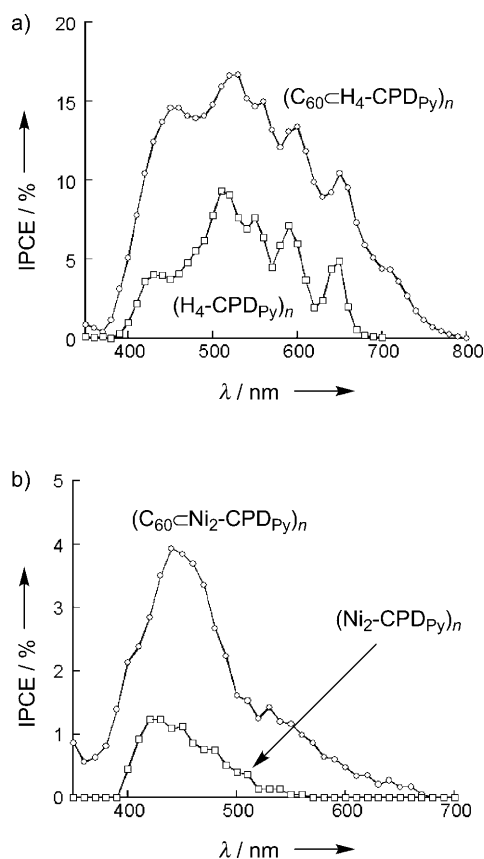


Figure 15. Photocurrent action spectra of a) the OTE/SnO₂/(C₆₀C₄H₄-CPD_{Py})_n electrode (line with circles) and the OTE/SnO₂/(H₄-CPD_{Py})_n electrode (line with squares), and b) the OTE/SnO₂/(C₆₀C₂Ni₂-CPD_{Py})_n electrode (line with circles) and the OTE/SnO₂/(Ni₂-CPD_{Py})_n electrode (line with squares). Electrolyte: 0.5 M LiI and 0.05 M I₂ in acetonitrile.

in which I_{sc} is the short-circuit photocurrent ($A\text{ cm}^{-2}$), W_{in} is the incident-light intensity ($W\text{ cm}^{-2}$), and λ is the wavelength (nm). The overall response of $(C_{60}\text{C}Ni_2\text{-CPD}_{Py})_n$ and $(C_{60}\text{C}H_4\text{-CPD}_{Py})_n$ on OTE/SnO₂ parallels the broad absorption spectral features (Figure 15), which indicates the in-

volvement of $(C_{60}\text{C}H_4\text{-CPD}_{Py})_n$ and $(C_{60}\text{C}Ni_2\text{-CPD}_{Py})_n$ in photocurrent generation. OTE/SnO₂/(C₆₀C₄H₄-CPD_{Py})_n gives rise to an especially broad photoresponse in the longer wavelength region (700–800 nm) because of the extended absorption of highly ordered clusters of C₆₀C₄H₄-CPD_{Py}. The maximum IPCE value for $(C_{60}\text{C}H_4\text{-CPD}_{Py})_n$ (17%) is much larger than that of $(C_{60}\text{C}Ni_2\text{-CPD}_{Py})_n$ (4%). This clearly indicates that the organized donor and acceptor alignment in $(C_{60}\text{C}Ni_2\text{-CPD}_{Py})_n$ enhances the IPCE.

We also evaluated the power characteristics of the OTE/SnO₂/(C₆₀C₄H₄-CPD_{Py})_n and OTE/SnO₂/(C₆₀C₂Ni₂-CPD_{Py})_n electrodes (Figure S12 in the Supporting Information). The power conversion efficiency, η , is calculated by using Equation (2).^[12j]

$$\eta = FF \times I_{sc} \times V_{oc} / W_{in} \quad (2)$$

in which the fill factor (FF) is defined as $FF = [IV]_{max} / I_{sc} V_{oc}$, in which V_{oc} is the open-circuit photovoltage, and I_{sc} is the short-circuit photocurrent. OTE/SnO₂/(C₆₀C₄H₄-CPD_{Py})_n has a fill factor of 0.40, an open-circuit voltage of 300 mV, a short-circuit current density of 1.10 mA cm⁻², and an overall power conversion efficiency (η) of 0.33% at an input power (W_{in}) of 40 mW cm⁻², whereas $FF = 0.34$, $V_{oc} = 160$ mV, and $I_{sc} = 0.148$ mA cm⁻² in the OTE/SnO₂/(C₆₀C₂Ni₂-CPD_{Py})_n. The η value of OTE/SnO₂/(C₆₀C₄H₄-CPD_{Py})_n (0.33%) is more than 16 times that of OTE/SnO₂/(C₆₀C₂Ni₂-CPD_{Py})_n (0.02%). Such a significant enhancement of the η value demonstrates that the strong ordering in the clusters and the efficient charge separation in $(C_{60}\text{C}H_4\text{-CPD}_{Py})_n$ improve the light-energy conversion properties.

Conclusion

We have reported the synthesis and crystal structure of a new porphyrin nanotube derived from the cyclic free-base porphyrin dimer H₄-CPD_{Py} with pyridyl substituents as self-assembling moieties. The tube is constructed through the stacking of the cyclic molecules through unique C–H···N hydrogen bonds and π – π interactions between the pyridyl groups in the crystal. The formation of the 1:1 inclusion complex of C₆₀ with H₄-CPD_{Py} (C₆₀C₄H₄-CPD_{Py}) was confirmed both in solution and in the crystal. Electrochemistry reveals that H₄-CPD_{Py} and C₆₀C₄H₄-CPD_{Py} have lower porphyrin oxidation potentials than those of Ni₂-CPD_{Py} and C₆₀C₂Ni₂-CPD_{Py}, which results in the lower energy level of the expected charge-separated state. The zigzag array of C₆₀ molecules is formed with van der Waals contacts between C₆₀ molecules inside the spaces surrounded by the porphyrin moieties in the crystal structure of C₆₀C₄H₄-CPD_{Py}. The formation of a charge-separated state of C₆₀C₄H₄-CPD_{Py} in the solid of C₆₀C₄H₄-CPD_{Py} was observed by using femtosecond laser flash photolysis. This result is different from that obtained with C₆₀C₂Ni₂-CPD_{Py}, and shows that it is possible to improve the efficiency of the charge separation by tuning

the electronic properties of the porphyrin moiety. An anisotropic charge mobility along the crystallographic *b* axis for the single crystal of C₆₀C₄H₄-CPD_{Py} was measured by FP-TRMC. The highest charge mobility was $\Sigma\mu=0.16$ and $0.13\text{ cm}^2\text{ V}^{-1}\text{ s}^{-1}$ along the zigzag array of C₆₀.

The photovoltaic activity of C₆₀C₄H₄-CPD_{Py} and C₆₀C₄H₄-CPD_{Py} was evaluated by constructing photoelectrochemical cells composed of modified electrodes and I⁻/I₃⁻ solution. C₆₀C₄H₄-CPD_{Py}-modified electrodes exhibited light-energy conversion properties, as represented by the IPCE value of 17% and the power conversion efficiency (η) of 0.33%. This indicates that the inclusion complexes of the self-assembling cyclic porphyrin dimers and fullerene C₆₀ are valid candidates for photovoltaic applications.

Experimental Section

Materials: All reagents and solvents were purchased from commercial suppliers as the best grade available, and were used without further purification unless otherwise noted. *o*-Dichlorobenzene was purified by distillation under reduced pressure after stirring over CaCl₂ for several days.

Instruments: ¹H and ¹³C NMR spectra were recorded on a JEOL JMX-GX400 (400 MHz) spectrometer. Chemical shifts were reported as δ values in ppm relative to tetramethylsilane. High-resolution fast atom bombardment MS (HR-FAB-MS) was performed on a JEOL LMS-HX-110 spectrometer with 3-nitrobenzyl alcohol (NBA) as the matrix. UV/Vis absorption and IR spectra were recorded on Shimadzu UV-3100PC and BIO RAD FTS6000 spectrophotometers, respectively. ESIMS was carried out on a Perkin-Elmer Sciex API 300 mass spectrometer. DPV and cyclic voltammetry were performed on a BAS 100B and ALS 630C potentiostat in a deaerated acetonitrile or *o*-dichlorobenzene/pyridine solution containing 0.10 M *n*Bu₄NPF₆ as the supporting electrolyte. The typical scan rate was 100 mV s⁻¹. A 6 mm diameter platinum electrode was used as the working electrode, while a platinum wire served as the counter electrode. An Ag/AgNO₃ electrode in acetonitrile or *o*-dichlorobenzene/pyridine, separated by a Vycor tip, was used as a reference. Redox potentials were determined with respect to that of the Fc⁺/Fc redox couple. All electrochemical measurements were carried out under an atmospheric pressure of argon.

Synthesis of 2: A solution of Zn(OAc)₂·2H₂O (excess) in methanol (120 mL) was added to a solution of 1^[18] (150 mg, 0.19 mmol) in CHCl₃ (300 mL) and heated at 65°C under N₂ overnight. The reaction mixture was diluted with CHCl₃ and washed with water (200 mL) twice. The organic layer was dried over Na₂SO₄ and the solvent was evaporated. The solid obtained was washed with hexane and dried in vacuo to give 2 as a purple powder (150 mg, 93%). ¹H NMR ([D₃]pyridine, 400 MHz): $\delta=0.31$ (s, 18H; -Si(CH₃)₃), 7.73 (t, *J*=7.7 Hz, 2H; Ar-H), 8.07 (d, *J*=7.8 Hz, 2H; Ar-H), 8.30 (d, *J*=4.4 Hz, 4H; Ar-H), 8.35 (d, *J*=7.6 Hz, 2H; Ar-H), 8.68 (s, 2H; Ar-H), 9.05 (d, *J*=4.6 Hz, 4H; pyrrole β -H), 9.11 (d, *J*=4.6 Hz, 4H; pyrrole β -H), 9.18 ppm (d, *J*=4.2 Hz, 4H; Ar-H); HR-FAB-MS (NBA): *m/z* calcd for C₅₂H₄₂N₆ZnSi₂: 870.2301; found: 870.2285; IR (KBr): $\tilde{\nu}=2958, 2156, 1593, 1404, 1340, 1250, 1072, 997, 931, 860, 795, 717\text{ cm}^{-1}$; UV/Vis (CHCl₃): λ_{max} (ϵ)=424 (477200), 553 (19600) 594 nm (4200 cm⁻¹ M⁻¹).

Synthesis of 3: A solution of potassium fluoride dehydrate (41 mg, 0.44 mmol) in DMF (4 mL) was added to 2 (87 mg, 0.1 mmol) under N₂ at room temperature. The solution was stirred overnight at room temperature. The reaction mixture was poured into water (40 mL) and filtered. The residue was washed with water and then methanol before being dried in vacuo to give 3 as a purple powder (61 mg, 85%). ¹H NMR ([D₃]pyridine, 400 MHz): $\delta=4.25$ (s, 2H; -C \equiv CH), 7.73 (t, *J*=7.7 Hz, 2H; Ar-H), 8.05 (d, *J*=8.1 Hz, 2H; Ar-H), 8.30 (d, *J*=4.2, 2H; Ar-H),

8.36 (d, *J*=7.6, 2H; Ar-H), 8.66 (s, 2H; Ar-H), 9.07 (d, *J*=4.6 Hz, 4H; pyrrole β -H), 9.11 (d, *J*=4.6 Hz, 4H; pyrrole β -H), 9.17 ppm (d, *J*=4.4, 4H; Ar-H); HR-FAB-MS (NBA): *m/z* calcd for C₄₆H₂₆N₆Zn: 726.1510; found: 726.1506; IR (KBr): $\tilde{\nu}=3280, 1599, 1340, 1203, 1076, 997, 924, 798\text{ cm}^{-1}$; UV/Vis (THF): λ_{max} (ϵ)=403 (48400), 423 (559600), 555 (22000), 595 nm (5400 cm⁻¹ M⁻¹).

Synthesis of H₂-CPD_{Py}: This compound was synthesized according to the literature^[36] with modification as follows. Cu^ICl (1.188 g, 12 mmol) was added to a solution of 3 (73 mg, 0.1 mmol) in pyridine (200 mL). The reaction mixture was stirred at 80°C for 24 h under air after which time it was diluted with CHCl₃ (200 mL), washed with aqueous ammonia (200 mL \times 3), dried over Na₂SO₄, and the solvent was evaporated. The purple residue was dissolved in pyridine (3 mL) again, and carefully acidified with a 6 N aqueous solution of HCl (aqueous, 40 mL). The green suspension was carefully poured into a saturated aqueous solution of NaHCO₃ (200 mL), and extracted with CHCl₃ (150 mL). The organic layer was dried over Na₂SO₄ and the solvent was evaporated. The residue was purified by flash column chromatography (CHCl₃/MeOH=150:1). After washing with methanol and drying in vacuo, the desired dimer (13 mg, 20%) together with the corresponding trimer (12 mg, 18%) were obtained as a reddish purple powder. ¹H NMR (CDCl₃, 400 MHz): $\delta=-3.01$ (brs, 4H; -NH) 7.32 (s, 4H; Ar-H) 7.72 (d, *J*=8.1 Hz, 4H; Ar-H), 7.80 (t, *J*=7.8, 4H; Ar-H), 7.95 (brs, 4H; Ar-H), 8.61 (d, *J*=7.6, 8H; Ar-H), 8.64 (d, *J*=4.9 Hz, 8H; pyrrole β -H), 8.67 (d, *J*=4.4 Hz, 8H; pyrrole β -H), 8.96 ppm (brs, 8H; Ar-H); HR-FAB-MS (NBA): *m/z* calcd for C₉₂H₅₂N₁₂: 1324.4438; found: 1324.4419; IR (KBr): $\tilde{\nu}=1593, 1473, 1402, 974, 881, 798, 727, 660\text{ cm}^{-1}$; UV/Vis (CHCl₃): λ_{max} (ϵ)=417 (742800), 515 (34000), 549 (10400), 588 (10800), 645 nm (4400 cm⁻¹ M⁻¹); elemental analysis calcd (%) for C₉₂H₅₂N₁₂·1.5C₆H₄Cl₂: C 78.47, H 3.78, N 10.87; found: C 78.84, H 3.95, N 10.89.

C₆₀C₄H₄-CPD_{Py}: ¹H NMR (CDCl₃/[D₆]benzene (1:1), 400 MHz): $\delta=-2.86$ (brs, 4H; -NH) 7.18 (s, 4H; Ar-H), 7.47–7.54 (m, 8H; Ar-H), 7.72–7.90 (brm, 8H; Ar-H), 8.47 (d, *J*=7.1 Hz, 4H; Ar-H), 8.58 (d, *J*=4.6 Hz, 8H; pyrrole β -H), 8.65 (d, *J*=4.9 Hz, 8H; pyrrole β -H), 8.84–8.99 ppm (brm, 8H; Ar-H); IR (KBr): $\tilde{\nu}=1591, 1473, 1400, 1082, 974, 796, 725, 577, 528\text{ cm}^{-1}$; elemental analysis calcd (%) for C₉₂H₅₂N₁₂·C₆₀·3C₇H₈·H₂O: C 88.78, H 3.36, N 7.18; found: C 88.98, H 3.33, N 7.23.

X-ray structure determination: X-ray crystallography was carried out on single crystals of H₂-CPD_{Py} and C₆₀C₄H₄-CPD_{Py} by using a Rigaku RAXIS imaging plate area detector with graphite monochromated Cu_{K α} radiation ($\lambda=1.54178\text{ \AA}$). The crystals were mounted on a glass fiber. To determine the cell constants and orientation matrix, three oscillation photographs were taken for each frame, with an oscillation angle of 3° and an exposure time of 3 min. Reflection data were corrected for both Lorentz and polarization effects. The structures were solved by direct methods (SIR-2004)^[37] with the Crystal Structure^[38] crystallographic software package, and refined by full-matrix least-squares procedures on *F*² for all reflections (SHELXL-97). Non-hydrogen atoms were refined anisotropically. Hydrogen atoms were refined by using the rigid model. The final structures were validated by using PLATON cif check. Summaries of the fundamental crystal data and experimental parameters for structure determination are given below.^[25]

Time-resolved transient absorption measurements: Femtosecond transient absorption spectroscopy was conducted by using an ultrafast source (Integra-C (Quantronix Corp.)), an optical parametric amplifier, TOPAS (Light Conversion), and a commercially available optical detection system, Helios, provided by Ultrafast Systems LLC. The source for the pump and probe pulses was derived from the fundamental output of Integra-C (780 nm, 2 mJ/pulse, and full-width at half-maximum (fwhm)) 130 fs) at a repetition rate of 1 kHz. 75% of the fundamental output of the laser was introduced into the TOPAS, which has optical frequency mixers that provide a tunable range from 285 to 1660 nm, while the rest of the output was used for white-light generation. Prior to generating the probe continuum, a variable neutral density filter was inserted in the path to generate a stable continuum. The laser pulse was then fed to a delay line that provides an experimental time window of 3.2 ns with a maximum step resolution of 7 fs. In our experiments, a wavelength at 420 nm of TOPAS output, which is the fourth harmonic of signal or idler

pulses, was chosen as the pump beam. As this TOPAS output consists of not only the desired wavelength but also unnecessary wavelengths, the latter (unwanted) output was deviated by using a wedge prism with a wedge angle of 18°. The desired beam was used to irradiate the sample with a spot size of 1 mm diameter, where it was merged with the white probe pulse in a close angle (<10°). The probe beam, after passing through the sample, was focused through a fiber-optic cable connected to a CCD spectrograph for recording the time-resolved spectra (420–1300 nm). Typically, 2500 excitation pulses were averaged over 5 s to obtain the transient spectrum at a set delay time. Kinetic traces at appropriate wavelengths were assembled from the time-resolved spectral data. All measurements were performed by using potassium bromide pellets that contained the ground powders of H₄-CPD_{Py} or C₆₀-CH₄-CPD_{Py} at 298 K.

FP-TRMC measurements: Nanosecond laser pulses from a Nd:yttrium + aluminum + garnet laser (second harmonic generation) (532 nm) from Spectra Physics, INDY-HG, full width at half maximum (5–8 ns) were used as excitation sources. The power density of the laser was set at 4.3–110 mJ cm⁻² (1.1–30 × 10¹⁶ photons cm⁻²). For time-resolved microwave conductivity (TRMC) measurements, the microwave frequency and power were set at approximately 9.1 GHz and 3 mW, respectively, so that the motion of the charge carriers was not disturbed by the low electric field of the microwaves. A Rohde & Schwarz SMA-100 A signal generator was used as a microwave continuum source. A crystal was mounted on a quartz rod with poly(vinylalcohol) binder, and set in the microwave cavity resonator (TE012 mode). The mounted crystal was back excited with a quartz rod, and rotated relative to the vector of the electric field in the cavity. The TRMC signal picked up by a diode (rise time <1 ns) was monitored by digital oscilloscope. All of the above experiments were carried out at room temperature. The transient photoconductivity ($\Delta\sigma$) of the samples is related to the reflected microwave power ($\Delta P_r/P_r$) and sum of the mobilities of charge carriers as given in Equations (3) and (4):

$$\langle \Delta\sigma \rangle = (1/A)(\Delta P_r/P_r) \quad (3)$$

$$\Delta\sigma = e\sum\mu\phi N \quad (4)$$

In these equations, A , e , ϕ , N , and $\sum\mu$ represent a sensitivity factor, the elementary charge of an electron, the photocarrier generation yield (quantum efficiency), the number of absorbed photons per unit volume, and the sum of mobilities for negative and positive carriers, respectively. The number of photons absorbed by the sample was estimated by measuring the transmitted power of laser pulses by an Ophir NOVA-display power meter and by the steady-state absorption spectrum of the film of C₆₀-CH₄-CPD_{Py} on a quartz substrate. Photoinduced current transients were recorded by using 0.2 μm-thick films coated onto interdigitated Au electrodes with a 5 μm gap in a vacuum chamber (<10⁻⁵ Pa) under excitation at 532 nm with a power density of around 4.8–7.2 mJ cm⁻². Current transients were predominantly observed under the applied bias of approximately 0.2–6.4 × 10⁴ V cm⁻¹, and were monitored by a Tektronic TDS 350 digitizing oscilloscope with the terminate resistance ranging from 3 kΩ and a Keithley R6487 current integrator. The transient current was also measured by using conventional DC current integration with a thin film sandwiched between Al and semitransparent Au electrodes under excitation at 532 nm with a power density of 16 mJ cm⁻². Other details of the apparatus are described elsewhere.^[23g–j]

Electron micrograph measurements: TEM measurements were recorded by applying a drop of the sample to a copper grid. Images were recorded on a Hitachi H 7100 transmission electron microscope at an accelerating voltage of 100 kV for imaging.

Preparation of dye-deposited OTE: The electrodes with C₆₀-CH₄-CPD_{Py}, H₄-CPD_{Py}, C₆₀-Ni₂-CPD_{Py}, Ni₂-CPD_{Py}, and C₆₀ were prepared by an electrochromic deposition method. The 125 μm suspension of these dyes in CHCl₃/o-dichlorobenzene/hexane (1:1:6, 2 mL) was transferred to a 1 cm cuvette in which two optically transparent electrodes were kept at a distance of 6 mm with a Teflon spacer. A direct current electric field (≈200 V cm⁻¹) was applied for 1 min between these two electrodes with a Power Pac HV (Bio-Rad). The OTE electrodes coated with C₆₀-CH₄-

CPD_{Py}, H₄-CPD_{Py}, C₆₀-Ni₂-CPD_{Py}, Ni₂-CPD_{Py} and C₆₀ are denoted as OTE/SnO₂/(C₆₀-CH₄-CPD_{Py})_n, OTE/SnO₂/(H₄-CPD_{Py})_n, OTE/SnO₂/(C₆₀-Ni₂-CPD_{Py})_n, OTE/SnO₂/(Ni₂-CPD_{Py})_n, and OTE/SnO₂/(C₆₀)_n, respectively.

Measurement of photoelectrochemical solar cells: Photoelectrochemical measurements were carried out in a standard two-compartment cell that consisted of a working electrode and a Pt wire gauze counter electrode in the electrolyte. The electrolyte was 0.5 M LiI and 0.05 M I₂ in acetonitrile. Keithley 2400 was used for recording photocurrent and photovoltage responses under an AM1.5 simulated light source (Otento-Sun II, Bunkoh-Keiki). For IPCE measurements, a monochromator (SM-25, Bunkoh-Keiki) was introduced into the path of the excitation beam (300 W xenon lamp, Bunkoh-Keiki) at the selected wavelength. The lamp intensity at each wavelength was determined by a Si photodiode (Hamamatsu Photonics S1337-1010BQ) and corrected.

Acknowledgements

This work was supported by Grants-in-Aid (Scientific Research on Innovative Areas No. 20108009 to F.T., “pi-Space”, and the Global COE Program, “Science for Future Molecular Systems”) from the Ministry of Education, Culture, Sports, Science and Technology of Japan, KOSEF/MEST through WCU project (R31-2008-000-10010-0), and by a Research Grant to F.T. from Tokuyama Science Foundation. H.N. acknowledges the Japan Society for the Promotion of Science (JSPS) for a Research Fellowship for Young Scientists.

- [1] a) *Fullerenes: Chemistry Physics and Technology* (Eds.: K. M. Kadish, R. S. Ruoff), Wiley, New York, **2000**; b) K. Ohkubo, S. Fukuzumi, *Bull. Chem. Soc. Jpn.* **2009**, *82*, 303–315; c) K. Ohkubo, S. Fukuzumi, *J. Porphyrins Phthalocyanines* **2008**, *12*, 993–1004; d) S. Fukuzumi, K. Ohkubo, H. Imahori, D. M. Guldi, *Chem. Eur. J.* **2003**, *9*, 1585–1593; e) S. Fukuzumi, I. Nakanishi, T. Suenobu, K. M. Kadish, *J. Am. Chem. Soc.* **1999**, *121*, 3468–3474.
- [2] a) B. C. Thompson, J. M. J. Fréchet, *Angew. Chem.* **2008**, *120*, 62–82; *Angew. Chem. Int. Ed.* **2008**, *47*, 58–77; b) A. R. Murphy, J. M. J. Fréchet, *Chem. Rev.* **2007**, *107*, 1066–1096.
- [3] E. Frankevich, Y. Maruyama, H. Ogata, *Chem. Phys. Lett.* **1993**, *214*, 39–44.
- [4] Y. Matsuo, E. Nakamura, *Chem. Rev.* **2008**, *108*, 3016–3028.
- [5] M. Makha, A. Purich, C. L. Raston, A. N. Sobolev, *Eur. J. Inorg. Chem.* **2006**, 507–517.
- [6] a) F. Diederich, M. Gómez-López, *Chem. Soc. Rev.* **1999**, *28*, 263–277; b) T. Haino, M. Yanase, Y. Fukazawa, *Angew. Chem.* **1998**, *110*, 1044–1046; *Angew. Chem. Int. Ed.* **1998**, *37*, 997–998.
- [7] P. D. W. Boyd, C. A. Reed, *Acc. Chem. Res.* **2005**, *38*, 235–242.
- [8] K. Tashiro, T. Aida, *Chem. Soc. Rev.* **2007**, *36*, 189–197.
- [9] a) D. Sun, F. S. Tham, C. A. Reed, L. Chaker, M. Burgess, P. D. W. Boyd, *J. Am. Chem. Soc.* **2000**, *122*, 10704–10705; b) D. Sun, F. S. Tham, C. A. Reed, L. Chaker, P. D. W. Boyd, *J. Am. Chem. Soc.* **2002**, *124*, 6604–6612.
- [10] a) D. Gust, T. A. Moore, *The Porphyrin Handbook*, Vol. 8 (Eds.: K. M. Kadish, K. M. Smith, R. Guilard), Academic Press, San Diego, **2000**, pp. 153–190; b) D. Gust, T. A. Moore, A. L. Moore, *Acc. Chem. Res.* **2001**, *34*, 40–48; c) S. Fukuzumi, D. M. Guldi, *Electron Transfer in Chemistry*, Vol. 2 (Eds.: V. Balzani), Wiley-VCH, Weinheim, **2001**, pp. 270–337; d) H. Imahori, S. Fukuzumi, *Adv. Funct. Mater.* **2004**, *14*, 525–536; e) P. V. Kamat, *J. Phys. Chem. C* **2007**, *111*, 2834–2860; f) F. D'Souza, O. Ito, *Coord. Chem. Rev.* **2005**, *249*, 1410–1422; g) S. Fukuzumi, *Org. Biomol. Chem.* **2003**, *1*, 609–620; h) S. Fukuzumi, *Bull. Chem. Soc. Jpn.* **2006**, *79*, 177–195.
- [11] H. Imahori, Y. Sekiguchi, Y. Kashiwagi, T. Sato, Y. Araki, O. Ito, H. Yamada, S. Fukuzumi, *Chem. Eur. J.* **2004**, *10*, 3184–3196.
- [12] a) T. Hasobe, H. Imahori, P. V. Kamat, S. Fukuzumi, *J. Am. Chem. Soc.* **2003**, *125*, 14962–14963; b) T. Hasobe, Y. Kashiwagi, M. A. Ab-

- salom, J. Sly, K. Hosomizu, M. J. Crossley, H. Imahori, P. V. Kamat, S. Fukuzumi, *Adv. Mater.* **2004**, *16*, 975–979; c) T. Hasobe, P. V. Kamat, V. Troiani, N. Solladié, T. K. Ahn, S. K. Kim, D. Kim, A. Kongkanand, S. Kuwabata, S. Fukuzumi, *J. Phys. Chem. B* **2005**, *109*, 19–23; d) T. Hasobe, H. Imahori, P. V. Kamat, T. K. Ahn, S. K. Kim, D. Kim, A. Fujimoto, T. Hirakawa, S. Fukuzumi, *J. Am. Chem. Soc.* **2005**, *127*, 1216–1228; e) T. Hasobe, K. Saito, P. V. Kamat, V. Troiani, H. Qiu, N. Solladié, K. S. Kim, J. K. Park, D. Kim, F. D'Souza, S. Fukuzumi, *J. Mater. Chem.* **2007**, *17*, 4160–4170; f) T. Hasobe, S. Fukuzumi, S. Hattori, P. V. Kamat, *Chem. Asian J.* **2007**, *2*, 265–272; g) T. Hasobe, S. Hattori, P. V. Kamat, S. Fukuzumi, *Tetrahedron* **2006**, *62*, 1937–1946; h) T. Hasobe, H. Murata, P. V. Kamat, *J. Phys. Chem. C* **2007**, *111*, 16626–16634; i) T. Hasobe, S. Hattori, P. V. Kamat, Y. Urano, N. Umezawa, T. Nagano, S. Fukuzumi, *Chem. Phys.* **2005**, *319*, 243–252; j) T. Hasobe, H. Imahori, S. Fukuzumi, P. V. Kamat, *J. Phys. Chem. B* **2003**, *107*, 12105–12112.
- [13] a) J. Y. Kim, K. Lee, N. E. Coates, D. Moses, T. Q. Nguyen, M. Dante, A. J. Heeger, *Science* **2007**, *317*, 222–225; b) G. Dennler, M. C. Scharber, C. J. Brabec, *Adv. Mater.* **2009**, *21*, 1323–1338; c) S. Günes, H. Neugebauer, N. S. Sariciftci, *Chem. Rev.* **2007**, *107*, 1324–1338.
- [14] a) M. Grätzel, *Inorg. Chem.* **2005**, *44*, 6841–6851; b) K. Tennakone, G. R. R. A. Kumara, I. R. M. Kottegoda, V. P. S. Perera, *Chem. Commun.* **1999**, 15–16; c) K. Hara, T. Horiguchi, T. Kinoshita, K. Sayama, H. Sugihara, H. Arakawa, *Sol. Energy Mater. Sol. Cells* **2000**, *64*, 115–134; d) Y. Shibano, T. Umeyama, Y. Matano, H. Imahori, *Org. Lett.* **2007**, *9*, 1971–1974.
- [15] a) P. V. Kamat, *J. Phys. Chem. C* **2008**, *112*, 18737–18753; b) H. J. Lee, J. H. Yum, H. C. Leventis, S. M. Zakeeruddin, S. A. Haque, P. Chen, S. I. Seok, M. Grätzel, M. K. Nazeeruddin, *J. Phys. Chem. C* **2008**, *112*, 11600–11608; c) I. Gur, N. A. Fromer, M. L. Geier, A. P. Alivisatos, *Science* **2005**, *310*, 462–465.
- [16] a) Y. Matsuo, Y. Sato, T. Niinomi, I. Soga, H. Tanaka, E. Nakamura, *J. Am. Chem. Soc.* **2009**, *131*, 16048–16050; b) J. S. Moon, J. K. Lee, S. Cho, J. Byun, A. J. Heeger, *Nano Lett.* **2009**, *9*, 230–234; c) H. Hoppe, N. S. Sariciftci, *J. Mater. Chem.* **2006**, *16*, 45–61; d) H. Hoppe, M. Niggemann, C. Winder, J. Kraut, R. Hiesgen, A. Hinsch, D. Meissner, N. S. Sariciftci, *Adv. Funct. Mater.* **2004**, *14*, 1005–1011.
- [17] A. Kira, T. Umeyama, Y. Matano, K. Yoshida, S. Isoda, J. K. Park, D. Kim, H. Imahori, *J. Am. Chem. Soc.* **2009**, *131*, 3198–3200.
- [18] H. Nobukuni, Y. Shimazaki, F. Tani, Y. Naruta, *Angew. Chem.* **2007**, *119*, 9133–9136; *Angew. Chem. Int. Ed.* **2007**, *46*, 8975–8978.
- [19] H. Nobukuni, F. Tani, Y. Shimazaki, Y. Naruta, K. Ohkubo, T. Nakanishi, T. Kojima, S. Fukuzumi, S. Seki, *J. Phys. Chem. C* **2009**, *113*, 19694–19699.
- [20] a) L. X. Chen, X. Zhang, E. C. Wasinger, K. Attenkofer, G. Jennings, A. Z. Muresan, J. S. Lindsey, *J. Am. Chem. Soc.* **2007**, *129*, 9616–9618; b) J. Rodriguez, D. Holten, *J. Chem. Phys.* **1989**, *91*, 3525–3531.
- [21] K. Mikami, S. Matsumoto, A. Ishida, S. Takamuku, T. Suenobu, S. Fukuzumi, *J. Am. Chem. Soc.* **1995**, *117*, 11134–11141.
- [22] a) C. A. Steren, H. van Willigen, L. Biczók, N. Gupta, H. Linschitz, *J. Phys. Chem.* **1996**, *100*, 8920–8926; b) J. W. Arbogast, C. S. Foote, M. Kao, *J. Am. Chem. Soc.* **1992**, *114*, 2277–2279.
- [23] a) J. M. Warman, M. P. de Haas, M. Grätzel, P. P. Infelta, *Nature* **1984**, *310*, 306–308; b) R. J. O. M. Hoofman, M. P. de Haas, L. D. A. Siebbeles, J. M. Warman, *Nature* **1998**, *392*, 54–56; c) J. M. Warman, M. P. de Haas, G. Dicker, F. C. Grozema, J. Piris, M. G. Debije, *Chem. Mater.* **2004**, *16*, 4600–4609; d) J. M. Warman, J. Piris, W. Pisula, M. Kastler, D. Wasserfallen, K. Müllen, *J. Am. Chem. Soc.* **2005**, *127*, 14257–14262; e) P. Prins, F. C. Grozema, J. M. Schins, S. Patil, U. Scherf, L. D. A. Siebbeles, *Phys. Rev. Lett.* **2006**, *96*, 146601–146601-4; f) P. A. C. Quist, J. Sweelssen, M. M. Koetse, T. J. Savenije, L. D. A. Siebbeles, *J. Phys. Chem. C* **2007**, *111*, 4452–4457; g) A. Acharya, S. Seki, A. Saeki, Y. Koizumi, S. Tagawa, *Chem. Phys. Lett.* **2005**, *404*, 356–360; h) H. Imahori, M. Ueda, S. Kang, H. Hayashi, S. Hayashi, H. Kaji, S. Seki, A. Saeki, S. Tagawa, T. Umeyama, Y. Matano, K. Yoshida, S. Isoda, M. Shiro, N. V. Tkachenko, H. Lemmetyinen, *Chem. Eur. J.* **2007**, *13*, 10182–10193; i) A. Saeki, S. Seki, T. Takenobu, Y. Iwasa, S. Tagawa, *Adv. Mater.* **2008**, *20*, 920–923; j) T. Amaya, S. Seki, T. Moriuchi, K. Nakamoto, T. Nakata, H. Sakane, A. Saeki, S. Tagawa, T. Hirao, *J. Am. Chem. Soc.* **2009**, *131*, 408–409.
- [24] H. L. Anderson, J. K. M. Sanders, *J. Chem. Soc. Chem. Commun.* **1989**, 1714–1715.
- [25] X-ray crystal structure data for H₄-CPD_{Py}: C₉₂H₅₂N₁₂·7(C₆H₄Cl₂); purple crystal; dimensions 0.47×0.16×0.10 mm³; triclinic; space group P $\bar{1}$; $a=14.8950(10)$, $b=14.9173(10)$, $c=15.5995(10)$ Å; $\alpha=68.737(4)$, $\beta=87.733(4)$, $\gamma=60.917(4)^\circ$; $V=2782.8(3)$ Å³; $Z=1$; $\rho_{\text{calcd}}=1.405$ g cm⁻³; $2\theta_{\text{max}}=136.46^\circ$; $T=133$ K; 28898 reflections collected; 9823 reflections used and 904 parameters. $R_1=0.0595$ ($I>2.0\sigma(I)$), $R_w=0.1302$ (all data). C₆₀·C₄H₄-CPD_{Py}: 2(C₉₂H₅₂N₁₂)·2(C₆₀)·H₂O; black crystal; crystal dimensions 0.68×0.08×0.05 mm³; monoclinic; space group C2/c; $a=54.3037(18)$, $b=15.0592(5)$, $c=35.6340(12)$ Å; $\beta=128.331(2)^\circ$; $V=22858.9(15)$ Å³; $Z=4$; $\rho_{\text{calcd}}=1.194$ g cm⁻³; $2\theta_{\text{max}}=136.50^\circ$; $T=133$ K; 130469 reflections collected; 20854 reflections used and 1539 parameters. $R_1=0.0540$ ($I>2.0\sigma(I)$), $R_w=0.1412$ (all data). CCDC-780017 and 780018 contain the supplementary crystallographic data for this paper. These data can be obtained free of charge from The Cambridge Crystallographic Data Centre via www.ccdc.cam.ac.uk/data_request/cif.
- [26] For experimental details, see the Supporting Information.
- [27] J. Y. Zheng, K. Tashiro, Y. Hirabayashi, K. Kinbara, K. Saigo, T. Aida, S. Sakamoto, K. Yamaguchi, *Angew. Chem.* **2001**, *113*, 1909–1913; *Angew. Chem. Int. Ed.* **2001**, *40*, 1857–1861.
- [28] a) H. Imahori, N. V. Tkachenko, V. Vehmanen, K. Tamaki, H. Lemmetyinen, Y. Sakata, S. Fukuzumi, *J. Phys. Chem. A* **2001**, *105*, 1750–1756; b) F. D'Souza, E. Maligaspe, P. A. Karr, A. L. Schumacher, M. E. Ojaimi, C. P. Gros, J. M. Barbe, K. Ohkubo, S. Fukuzumi, *Chem. Eur. J.* **2008**, *14*, 674–681.
- [29] N. V. Tkachenko, H. Lemmetyinen, J. Sonoda, K. Ohkubo, T. Sato, H. Imahori, S. Fukuzumi, *J. Phys. Chem. A* **2003**, *107*, 8834–8844.
- [30] J. P. Bourgeois, F. Diederich, L. Echegoyen, J. F. Nierengarten, *Helv. Chim. Acta* **1998**, *81*, 1835–1844.
- [31] PLATON, a multipurpose crystallographic tool: A. L. Spek, *J. Appl. Crystallogr.* **2003**, *36*, 7–13.
- [32] S. Fukuzumi, T. Suenobu, M. Patz, T. Hirasaka, S. Itoh, M. Fujitsuka, O. Ito, *J. Am. Chem. Soc.* **1998**, *120*, 8060–8068.
- [33] H₄-CPD_{Py} shows a steady-state fluorescence spectrum with a peak at 649 nm (Figure S7 in the Supporting Information). The singlet excited energy is determined from the absorption and fluorescence maxima.
- [34] J. W. Arbogast, A. P. Darmanyan, C. S. Foote, Y. Rubin, F. N. Diederich, M. M. Alvarez, S. J. Anz, R. L. Whetten, *J. Phys. Chem.* **1991**, *95*, 11–12.
- [35] The value of ϕ determined by the DC-CI experiment under high electric field strength is probably overestimated. Therefore, the actual value of the mobilities may be larger than determined in this study.
- [36] a) H. L. Anderson, J. K. M. Sanders, *Angew. Chem.* **1990**, *102*, 1478–1480; *Angew. Chem. Int. Ed. Engl.* **1990**, *29*, 1400–1403; b) H. L. Anderson, J. K. M. Sanders, *J. Chem. Soc. Perkin Trans. 1* **1995**, 2223–2229; c) H. J. Kim, J. E. Redman, M. Nakash, N. Feeder, S. J. Teat, J. K. M. Sanders, *Inorg. Chem.* **1999**, *38*, 5178–5183.
- [37] M. C. Burla, R. Caliendo, M. Camalli, B. Carrozzini, G. L. Cascara-no, L. De Caro, C. Giacovazzo, G. Polidori, R. Spagna, *J. Appl. Crystallogr.* **2005**, *38*, 381–388.
- [38] Crystal structure analysis software, crystal structure 3. 8. 2, Rigaku/ MSC, The Woodlands, USA, Rigaku, Japan.

Received: June 28, 2010
Published online: August 30, 2010